Journal of ELECTRONIC MATERIALS, Vol. 42, No. 7, 2013
DOI: 10.1007/s11664-012-2407-9

A TEG Efficiency Booster with Buck–Boost Conversion

HONGFEI WU,[1,3] KAI SUN,[2] JUNJUN ZHANG,[1] and YAN XING[1]

1.—Jiangsu Key Lab of New Energy Generation, Nanjing University of Aeronautics & Astronautics, Nanjing 210016, China. 2.—State Key Lab of Power Systems, Department of Electrical Engineering, Tsinghua University, Beijing 100084, China. 3.—e-mail: wuhongfei@nuaa.edu.cn

A thermoelectric generator (TEG) efficiency booster with buck–boost conversion and power management is proposed as a TEG battery power conditioner suitable for a wide TEG output voltage range. An inverse-coupled inductor is employed in the buck–boost converter, which is used to achieve smooth current with low ripple on both the TEG and battery sides. Furthermore, benefiting from the magnetic flux counteraction of the two windings on the coupled inductor, the core size and power losses of the filter inductor are reduced, which can achieve both high efficiency and high power density. A power management strategy is proposed for this power conditioning system, which involves maximum power point tracking (MPPT), battery voltage control, and battery current control. A control method is employed to ensure smooth switching among different working modes. A modified MPPT control algorithm with improved dynamic and steady-state characteristics is presented and applied to the TEG battery power conditioning system to maximize energy harvesting. A 500-W prototype has been built, and experimental tests carried out on it. The power efficiency of the prototype at full load is higher than 96%, and peak efficiency of 99% is attained.

Key words: Thermoelectric, buck–boost conversion, maximum power point tracking, power management

INTRODUCTION

Thermoelectric generators (TEGs), which can directly convert thermal energy into electric power, have recently attracted increasing attention as a clean renewable energy source.[1,2] A TEG-based waste heat recovery system can improve the overall system efficiency for some applications where a large amount of energy cannot be recycled and is wasted in the form of exhausted heat.[3–8] However, the thermal–electric energy conversion efficiency of TEGs is low due to the limitations of thermoelectric materials. To maximize energy harvesting, high-conversion-efficiency power converters along with maximum power point tracking (MPPT) techniques are needed.

A TEG module can be characterized as a TEG voltage source and an inner impedance. The inner impedance changes dynamically with the temperature difference between its hot side and cold side.[9–11] The equivalent circuit for a TEG and its power–voltage and current–voltage curves are illustrated in Fig. 1.

With a constant temperature difference, the source voltage e_t and inner resistance r_t can be treated as constant values. However, when the temperature difference varies, both e_t and r_t change dynamically in a wide range. Thus, a power converter with step-up/down capability, which can adapt to the wide TEG output voltage range, is required for the TEG. Many step-up/down power converters have been proposed for various applications.[12] However, traditional single-switch step-up/down converters, such as buck–boost, Cuk, Zeta, and SEPIC converters, suffer from high device stresses, large filter volume, discontinuous input/output currents, opposite input/output voltage polarity, etc. An H-bridge buck–boost converter can work as either a buck or

(Received July 5, 2012; accepted December 26, 2012; published online February 5, 2013)

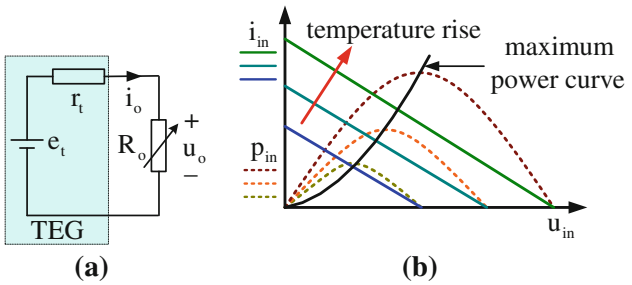

Fig. 1. Equivalent circuit and output characteristics of a TEG: (a) equivalent circuit, (b) output characteristics.

boost converter with a simple topology and flexible control scheme,[13–15] but the input/output current is discontinuous and a large filter capacitor is required. A boost-cascaded-buck converter has been applied to TEG power systems.[16,17] Both the input and output currents of this converter are continuous thanks to the input and output filter inductors. As a result, double-layer capacitors with small capacitance can be employed to improve the reliability of the system. However, two bulky filter inductors have to be used in this converter, which lowers the power density and increases the cost and size of the converter. To overcome these drawbacks, in this paper, a boost-cascaded-buck converter with a coupled inductor is proposed for the TEG battery power conditioning system.

Many schemes have been proposed to implement MPPT in photovoltaic applications. Among them, the perturbation and observation (P&O) method is the most popular method for its simplicity, ease of implementation, and good performance. This method can be directly applied to TEG power systems.[18–21] However, the traditional P&O method with a fixed perturbation step suffers from several demerits. The oscillations are proportional to the perturbation steps. A larger perturbation step can improve the dynamic performance but leads to larger oscillations in the steady state. Hence, a tradeoff between faster dynamic response and smaller steady-state oscillation is inherent. Many improved P&O methods have been proposed for photovoltaic applications. Note that the output characteristics of photovoltaic and TEG devices are different. In this paper, a modified MPPT method is proposed to improve the dynamic and steady-state performance based on the analysis of TEG characteristics.

The objective of this paper is to propose a TEG efficiency booster with buck–boost conversion that can satisfy the wide output voltage range of TEGs. A buck–boost converter with coupled inductor (BBC-CI), its power management strategy, and a modified MPPT method are proposed for the TEG battery power conditioning system.

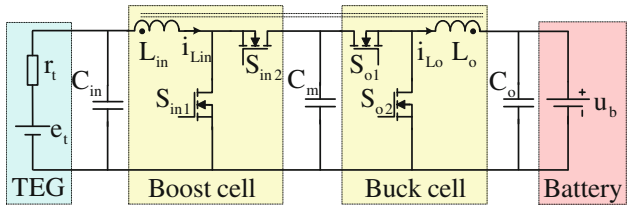

Fig. 2. Boost–buck converter with a coupled inductor.

ANALYSIS AND DESIGN OF THE POWER STAGE

Buck–Boost Topology

To interface with the TEG module, which has a wide output voltage range, a boost–buck converter with a coupled inductor (BBC-CI) is presented to meet the demands of battery charging applications, as shown in Fig. 2. The input stage of the BBC-CI is a boost switching cell, while the output stage is a buck switching cell. The inductors of the two cells, L_{in} and L_o, are negatively coupled via a common magnetic core. Thus, only one magnetic core is needed, and the direct-current (DC) bias of the core can be reduced effectively, which can help to reduce the size of the inductor and improve the power density of the converter.

Since both the input and output sides have their own filter inductor, the input and output current of the BBC-CI are continuous. Therefore, all the filter capacitors, C_{in}, C_m, and C_o, can be implemented with multilayer ceramic capacitors.

Operation Principles

The BBC-CI can operate in either boost or buck mode. When it operates in the boost mode, S_{o1} is always on and S_{o2} always off, and the converter features a boost converter with a C–L–C-type output filter. When it operates in the buck mode, S_{in1} is always off and S_{in2} always on, and the converter features a buck converter with a C–L–C-type input filter. The equivalent circuits of the BBC-CI in the boost mode and buck mode are shown in Figs. 3a and b, respectively. Figure 4 shows the key waveforms of the BBC-CI in the two modes, where u_{GSin1} and u_{GSo1} are the driving signals of S_{in1} and S_{o1}, I_{Lin} and I_{Lo} are the currents flowing through L_{in} and L_o, and Φ_{Lin} and Φ_o are the magnetic fluxes generated by I_{Lin} and I_{Lo}. The total magnetic flux Φ_L through the core is $\Phi_{Lin} - \Phi_{Lo}$, which is much less than Φ_{Lin} or Φ_{Lo}.

Figure 5 gives the equivalent circuit of the negatively coupled inductor, where the coupled inductor is modeled as an ideal transformer (turns ratio 1:n), a magnetizing inductor L_m, and a leakage inductor L_k. Denoting the mutual inductance by M and the coupling coefficient by k, we have

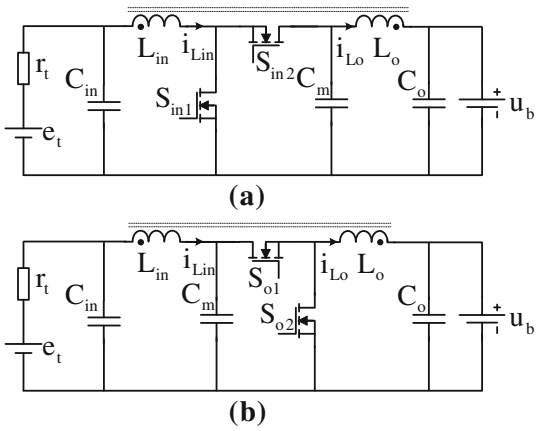

Fig. 3. Equivalent circuits of the BBC-CI in (a) boost mode, and (b) buck mode.

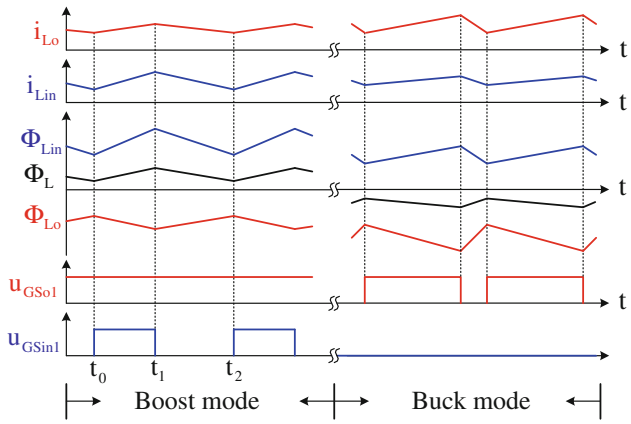

Fig. 4. Key waveforms of the BBC-CI.

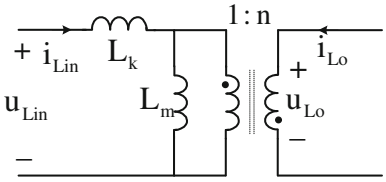

Fig. 5. Equivalent circuit model of the coupled inductor.

$$\begin{cases} k = \dfrac{M}{\sqrt{L_{\text{in}}L_{\text{o}}}}, \\ L_k = (1-k^2)L_{\text{in}}, \\ L_{\text{m}} = k^2 L_{\text{in}}. \end{cases} \tag{1}$$

The voltage of the two coupled inductors can be given by

$$\begin{cases} u_{\text{Lin}} = L_{\text{in}}\mathrm{d}i_{\text{Lin}}/\mathrm{d}t - M\mathrm{d}i_{\text{Lo}}/\mathrm{d}t, \\ u_{\text{Lo}} = L_{\text{o}}\mathrm{d}i_{\text{Lo}}/\mathrm{d}t - M\mathrm{d}i_{\text{Lo}}/\mathrm{d}t. \end{cases} \tag{2}$$

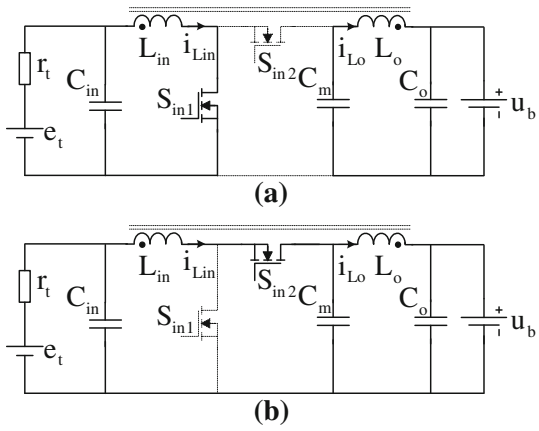

Fig. 6. Equivalent circuits of boost mode: (a) state I, and (b) state II.

Take the boost mode as an example for analysis. There are two switching states in one switching cycle. The equivalent circuits of the different states are shown in Fig. 6.

State I [t_0 to t_1] (Fig. 6a): At t_0, S_{in1} is turned on and S_{in2} is turned off. The inductor currents i_{Lin} and i_{Lo} increase linearly.

$$\begin{cases} \mathrm{d}i_{\text{Lin}}/\mathrm{d}t = u_{\text{in}}/[L_{\text{in}}(1-k^2)], \\ \mathrm{d}i_{\text{Lo}}/\mathrm{d}t = nku_{\text{in}}/[L_{\text{o}}(1-k^2)]. \end{cases} \tag{3}$$

where u_{in} is the input voltage of the BBC-CI

State II [t_1 to t_2] (Fig. 6b): At t_1, S_{in1} is turned off and S_{in2} is turned on. The inductor currents i_{Lin} and i_{Lo} decrease linearly.

$$\begin{cases} \mathrm{d}i_{\text{Lin}}/\mathrm{d}t = (u_{\text{in}}-u_{\text{b}})/[L_{\text{in}}(1-k^2)], \\ \mathrm{d}i_{\text{Lo}}/\mathrm{d}t = nk(u_{\text{in}}-u_{\text{b}})/[L_{\text{o}}(1-k^2)]. \end{cases} \tag{4}$$

where u_{b} is the output voltage of the BBC-CI

Denote the duty cycle of S_{in1} and S_{o1} as D_{in} and D_{o}, respectively. According to Eqs. (3) and (4), the inductor current ripples, Δi_{Lin} and Δi_{Lo}, in the boost mode can be obtained as

$$\begin{cases} \Delta i_{\text{Lin}} = u_{\text{o}}T_{\text{s}}D_{\text{in}}(1-D_{\text{in}})/[L_{\text{in}}(1-k^2)], \\ \Delta i_{\text{Lo}} = nku_{\text{o}}T_{\text{s}}D_1(1-D_1)/[L_{\text{o}}(1-k^2)], \end{cases} \tag{5}$$

where T_{s} is the switching period.

By following similar analysis processes, the current ripples in the buck mode can also be obtained as

$$\begin{cases} \Delta i_{\text{Lin}} = ku_{\text{b}}T_{\text{s}}(1-D_{\text{o}})/[nL_{\text{in}}(1-k^2)], \\ \Delta i_{\text{Lo}} = u_{\text{b}}T_{\text{s}}(1-D_{\text{o}})/[L_{\text{o}}(1-k^2)]. \end{cases} \tag{6}$$

Design Consideration of the Coupled Inductor

Using $u_{\text{b}}T_{\text{s}}/L_{\text{in}}$ to normalize Δi_{Lin} and $u_{\text{b}}T_{\text{s}}/L_{\text{o}}$ to normalize Δi_{Lo}, the normalized current ripple can be given as

$$\Delta i_{\mathrm{Lin\_nor}} = \begin{cases} k_{\mathrm{io}}(1-k_{\mathrm{io}})/(1-k^2) \text{ when } k_{\mathrm{io}} \le 1 \\ k(1-1/k_{\mathrm{io}})/[n(1-k^2)] \text{ when } k_{\mathrm{io}} > 1 \end{cases} \tag{7}$$

$$\Delta i_{\mathrm{Lo\_nor}} = \begin{cases} nkk_{\mathrm{io}}(1-k_{\mathrm{io}})/(1-k^2) \text{ when } k_{\mathrm{io}} \le 1 \\ (1-1/k_{\mathrm{io}})/(1-k^2) \text{ when } k_{\mathrm{io}} > 1 \end{cases} \tag{8}$$

In Eqs. (7) and (8), $k_{\mathrm{io}} = u_{\mathrm{in}}/u_{\mathrm{b}}$.

Assume the turns ration $n = 1$, the normalized current ripples versus the conversion ratio K_{io}, with different coupling coefficients, are shown in Fig. 7. It can be seen that the current ripples increase with increase of the coupling coefficient. When $k < 0.4$, the increment of the current ripple is slight.

As illustrated in Fig. 7, when the converter operates in the boost mode, a current ripple will reflect to the output side through the coupling inductor and vice versa. When selecting the coupling coefficient of the inductor, the following principle can be obeyed: the maximum current ripple of L_{in} in the buck mode should be smaller than that in the boost mode, and the maximum current ripple of L_{o} in the boost mode should be smaller than that in the buck mode.

Pulse Width Modulation

A two-carrier-based pulse width modulation scheme is applied to the BBC-CI, as shown in Fig. 8. In Fig. 8, u_{tri1} and u_{tri2} are the two carriers, and u_{ctrl} is the control voltage shared by the two carriers. The valley value of u_{tri1} equals the peak value of u_{tri2}. When $u_{\mathrm{in}} < u_{\mathrm{b}}$, u_{ctrl} intersects with u_{tri1} and the converter works in the boost mode. When $u_{\mathrm{in}} > u_{\mathrm{b}}$, u_{ctrl} intersects with u_{tri2} and the converter works in the buck mode. When the input voltage varies, the converter is able to switch between the boost mode and the buck mode smoothly.

CONTROL ALGORITHM OF THE TEG BATTERY POWER CONDITIONING SYSTEM

Control Algorithm

Figure 9 shows the proposed control diagram of the TEG battery power conditioning system. The controller has only one PI regulator and can achieve MPPT control, battery voltage control, and battery current control, simultaneously. The battery charging strategy is shown in Fig. 10. The power conditioning system has three possible working modes, namely MPPT mode, constant current mode, and constant voltage mode. As shown in Fig. 10, when the TEG module cannot provide enough power and the battery charging current and charging voltage are lower than the maximum values, the system works in the MPPT mode. Once the charging voltage or charging current reaches the maximum value and the battery cannot absorb the maximum power supplied by the TEG module, the system will switch to the constant voltage mode or the constant current mode.

The work mode is determined by the power conditions such as the available TEG power and the state of charge (SoC) of the battery. In order to implement smooth work mode transitions, a seamless mode transition controller is proposed by employing a competitive algorithm, as shown in Fig. 9. u_{inr}, which is provided by the MPPT controller, is the reference for the input voltage, while i_{br} and u_{br} are the references for the maximum

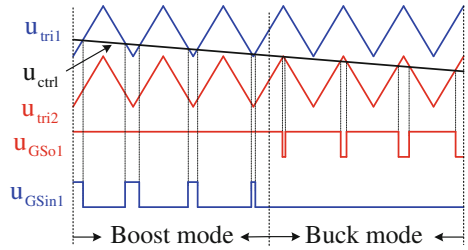

Fig. 8. Pulse width modulation scheme.

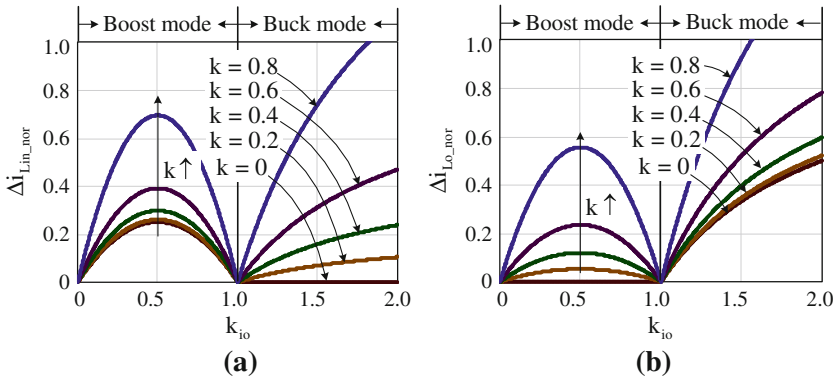

Fig. 7. Current ripples versus conversion ratio: (a) $\Delta i_{\mathrm{Lin\_nor}}$, and (b) $\Delta i_{\mathrm{Lo\_nor}}$.

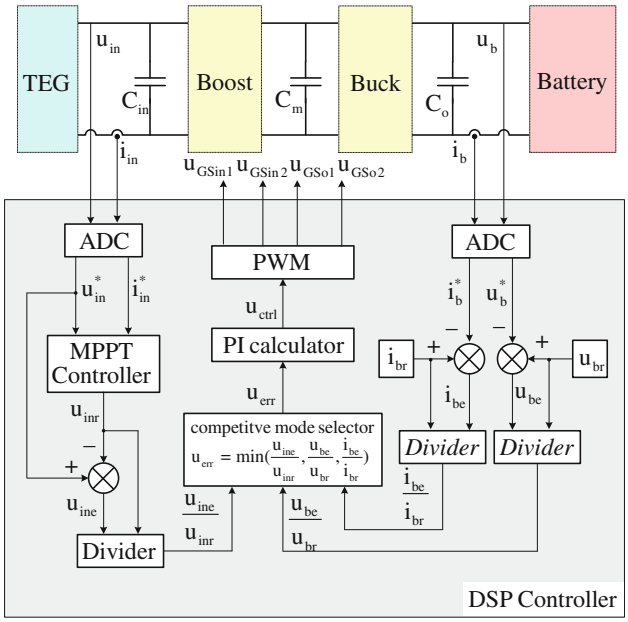

Fig. 9. Control diagram of the TEG battery power conditioning system. PI = Proportional-Integral, ADC = Analog to Digital Converter, DSP = Digital Signal Processor.

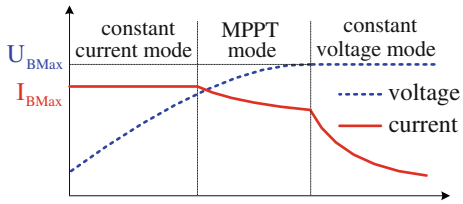

Fig. 10. Battery charging strategy.

battery charging current and the maximum battery charging voltage. u_{ine}, u_{be}, and i_{be} are three errors, being calculated by the following equations:

$$\begin{cases} u_{ine} = u_{in}^{*} - u_{inr} \\ i_{be} = i_{br} - i_{b}^{*} \\ u_{be} = u_{br} - u_{b}^{*}. \end{cases} \tag{9}$$

where u_{in}^{*}, i_{b}^{*}, and u_{b}^{*} are the sampled values of the input voltage u_{in}, battery current i_b, and battery voltage u_b. All three errors, u_{ine}, u_{be}, and i_{be}, are normalized by their references, u_{inr}, u_{br}, and i_{br}, respectively. Then, the minimum value among the three normalized errors is selected as the input to the PI regulator. Thus, the input of the PI regulator, u_{err}, is derived from the following equation:

$$u_{err} = \min\left(\frac{u_{ine}}{u_{inr}}, \frac{u_{be}}{u_{br}}, \frac{i_{be}}{i_{br}}\right). \tag{10}$$

According to (10), when the output power of the TEG is insufficient to make u_b or i_b reach the maximum value, the battery charging voltage u_b and charging current i_b are smaller than the reference values, and u_{be} and i_{be} will be greater than zero. In this scenario, u_{ine} will equal zero, which makes (u_{ine}/u_{inr}) the minimum value and $u_{err} = (u_{ine}/u_{inr})$. As a result, the input voltage will be under control and the system works in the MPPT mode. Once u_b or i_b reaches the maximum value, u_{be} or i_{be} will decrease to zero and make the system switch to the constant voltage mode or constant current mode automatically. Because all three control loops share only one PI regulator, the converter is always under control of this PI regulator, and there is no dead zone or response time during mode transitions. Hence, seamless mode transitions can be realized with the proposed control algorithm.

Modified P&O MPPT Algorithm

Perturb and observe (P&O) methods have been widely used in photovoltaic power systems for MPPT due to their simplicity, ease of implementation, and good performance. To overcome the drawbacks of the traditional P&O method, which uses a fixed perturbation step, and attempt to improve the dynamic and steady-state performance, a modified P&O MPPT algorithm is applied to the TEG battery power condition system.

As mentioned above, a TEG electrical model can be simplified as a voltage source e_t in series with an inner resistance r_t. Assuming the input voltage of the BBC-CI is u_{in}, the input power of the converter can be given by

$$p_{in} = \frac{u_{in}(e_t - u_{in})}{r_t}. \tag{11}$$

According to (11), the maximum input power p_{inmax} occurs when $u_{in} = e_t/2$, i.e.,

$$p_{inmax} = \frac{e_t^2}{4r_t}. \tag{12}$$

The power curve of the TEG shows that the derivative of p_{in} is positive before reaching the MPP, zero at the MPP, and negative after passing the MPP. On the other hand, according to (11), we have

$$\frac{dp_{in}}{du_{in}} = \frac{e_t - 2u_{in}}{r_t}, \begin{cases} >0, & \text{before MPP} \\ <0, & \text{after MPP} \end{cases} \tag{13}$$

To track the MPP, the following behaviors are required: (1) increase u_{in} when $(dp_{in}/du_{in}) > 0$, (2) decrease u_{in} when $(dp_{in}/du_{in}) < 0$.

On the other hand, according to Eq. (13), (dp_{in}/du_{in}) is proportional to the distance between the operation point and the MPP. Therefore, to improve the dynamic performance of MPPT, the perturbation step of the input voltage can be proportional to (dp_{in}/du_{in}), which is

$$\Delta u_{in\_step} = k \cdot \frac{dp_{in}}{du_{in}}, \tag{14}$$

where k is a positive constant value. It is obvious that $(dp_{in}/du_{in}) > 0$, $\Delta u_{in\_step} > 0$, and $(dp_{in}/du_{in}) < 0$, $\Delta u_{in\_step} < 0$ are the same as the behaviors required by the MPPT process. Therefore, the discrete-time expression of the MPPT scheme is written as

$$u_{inr}[n+1] = u_{inr}[n] + \Delta u_{in\_step}[n+1], \quad (15)$$

$$\Delta u_{in\_step}[n+1] = k \cdot \frac{\Delta p_{in}[n]}{\Delta u_{in\_step}[n]}, \quad (16)$$

where $[n + 1]$ and $[n]$ represent the quantized values at the $(n + 1)$th and nth sampling intervals, respectively.

Based on this analysis, the flowchart of the modified P&O MPPT algorithm is shown in Fig. 11. Large perturbation steps are applied to reach the MPP quickly when the operation point is far from the MPP, and as the MPP is approached, the perturbation step is correspondingly decreased to avoid large oscillations around the maximum power operating point. As a result, both the dynamic and steady-state performance can be improved.

EXPERIMENTAL RESULTS

A 500-W BBC-CI prototype was built and tested to verify the effectiveness of the power stage and proposed control strategies. The key parameters are as follows: u_{in} = 8 V to 32 V, u_b = 20 V to 28 V, L_{in} = 19.5 μH, L_o = 28.8 μH, coupling coefficient of L_o and L_{in} = 0.35, and switching frequency = 80 kHz. The TEG is emulated by a DC voltage source in series with a variable resistor.

The steady-state waveforms of the BBC-CI in the boost and the buck mode are shown in Fig. 12. Figure 12a is measured with 16 V input voltage and 125 W output power, while Fig. 12b is measured with 32 V input voltage and 500 W output power. It can be seen that, with the coupled inductor, both the input current and output current are continuous independent of whether the BBC-CI operates in the boost mode or the buck mode. The experimental waveforms accord with the theoretical analysis well.

The start-up process was tested, and the waveforms are shown in Fig. 13. It can be seen that the converter can reach the maximum power point very quickly, and once there, the perturbation steps are very small and the voltage oscillation is also very small. It has been verified that the modified MPPT strategy can achieve good dynamic and steady-state performance.

To verify the smooth transitions between different working modes, the BBC-CI was tested with a resistance load. As a result, the output voltage and current can be changed by adjusting the load resistance. The working mode transition waveforms are shown in Fig. 14. Figure 14a shows the measured results when the working mode changes from the MPPT mode to the constant voltage mode. The load is reduced by increasing the load resistance. Before the load reduction, the output voltage u_b is less than its command of 28 V, and thus the controller operates in the MPPT mode. After the load is reduced, u_b reaches its command and the working mode is switched to the constant voltage mode. The working mode is returned to the MPPT mode again

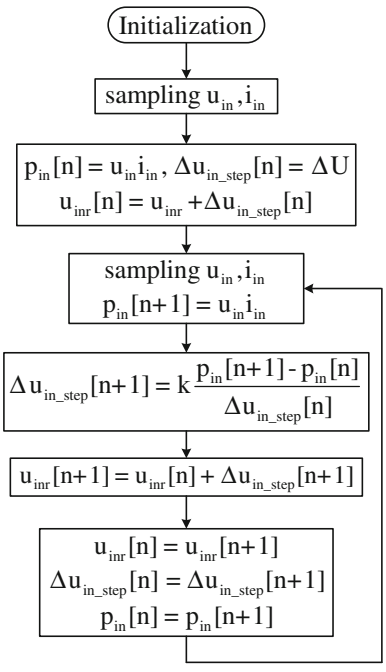

Fig. 11. Flowchart of the modified P&O MPPT algorithm.

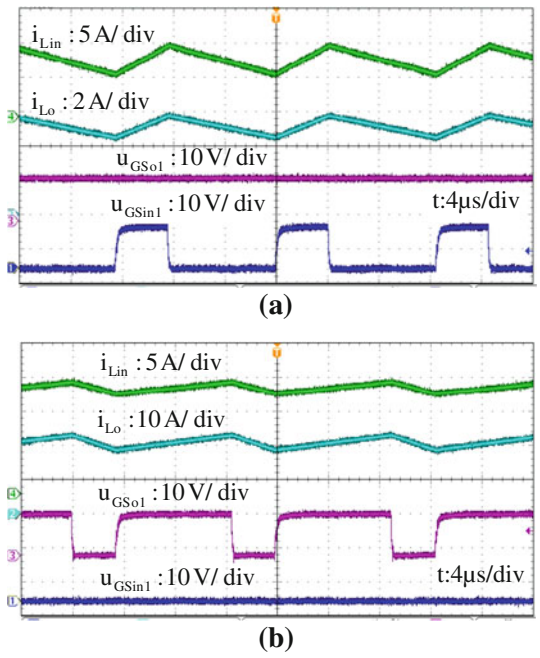

Fig. 12. Steady-state waveforms in: (a) boost mode, and (b) buck mode.

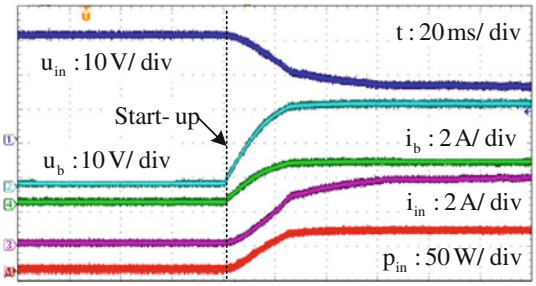

Fig. 13. Start-up waveforms.

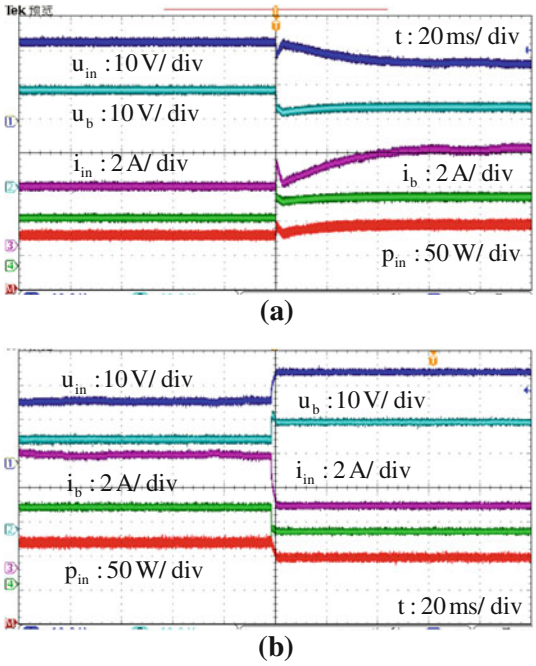

Fig. 14. Working mode transition waveforms: (a) MPPT mode to constant voltage mode, and (b) constant voltage mode to MPPT mode.

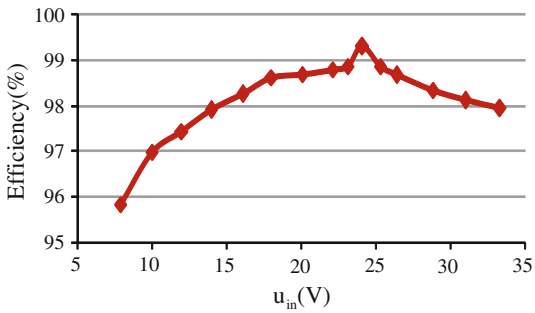

Fig. 15. Efficiency versus input voltage of BBC-CI.

when the load is increased by decreasing the load resistance, as shown in Fig. 14b.

The efficiency curve of the BBC-CI over the whole input voltage range at full load is shown in Fig. 15. The battery voltage is 24 V. When the input voltage is lower than 24 V, the converter operates in the boost mode, and when the input voltage is higher than 24 V, the converter operates in the buck mode. It can be seen that high conversion efficiency over the whole input voltage range has been achieved by using the BBC-CI.

CONCLUSIONS

In this paper, a boost–buck converter with coupled inductor (BBC-CI) is adopted for a high-efficiency TEG battery power conditioning system to operate over a wide input voltage range and maximize the TEG output power. An inverse-coupled inductor is employed in the BBC-CI to achieve smooth current and power with low ripples on both the TEG and battery sides. A power management strategy integrating MPPT, battery voltage control, and battery current control is proposed, which employs competitive logic to determine the control commands. Using this strategy, smooth mode transitions are achieved. A modified perturbation and observation MPPT method is employed to maximize the output power of the TEG, which improves both the dynamic and steady-state performance.

Experimental results on a 500-W BBC-CI prototype verify the feasibility and effectiveness of the power stage and the proposed control strategies for the TEG power conditioning system.

ACKNOWLEDGEMENTS

The authors would like to acknowledge support from the Tsinghua University Initiative Scientific Research Program (20101081909), by the State Key Lab of Power Systems, Tsinghua University under Grant Nos. SKLD10KM02 and SKLD10M09, and a project funded by the Priority Academic Program Development of Jiangsu Higher Education Institutions.

REFERENCES

1. L. Miao, M. Zhang, S. Tanemura, T. Tanaka, Y.P. Kang, and G. Xu, *J. Electron. Mater.* 41, 1759 (2012).
2. L.A. Rosendahl, P.V. Mortensen, and A.A. Enkeshafi, *J. Electron. Mater.* 40, 1111 (2011).
3. J. Gao, K. Sun, L. Ni, M. Chen, Z. Kang, L. Zhang, Y. Xing, and J. Zhang, *J. Electron. Mater.* 41, 1043 (2012).
4. K. Yazawa and A. Shakouri, *J. Electron. Mater.* 41, 1845 (2012).
5. C.Q. Su, W.W. Zhan, and S. Shen, *J. Electron. Mater.* 41, 1693 (2012).
6. Y.D. Deng, W. Fan, K. Ling, C.Q. Su, *J. Electron. Mater.* 41, 1698, (2012).
7. J. LaGrandeur, D. Crane, S. Hung, B. Mazar, A. Eder, *Proceedings of 25th Int. Conf. Thermoelect.* (2006), pp.343 - 348.
8. X. Zhang, K.T. Chau, and C.D. Chan, *J. Asian Electr. Vehicles.* 2, 1119 (2008).
9. L. Chen, D. Cao, Y. Huang, F. Peng, *Proceedings of 39th IEEE Power Electron.*(2008), pp.1098 - 1103.
10. S. Lineykin and S. Ben-Yaakov, *IEEE Trans. Ind. Appl.* 43, 505 (2007).
11. J. Zhu, J. Gao, M. Chen, J. Zhang, Q. Du, L.A. Rosendahl, and R.O. Suzuki, *J. Electron. Mater.* 40, 744 (2011).
12. H. Cheng and K.M. Smedley, *IEEE T. Power Electr.* 25, 280 (2010).
13. H. Nagayoshi, K. Tokumisum and T. Kajikawa, *Proceedings of 26th Int. Conf. Thermoelect.* (2007), pp. 318-321.

14. P.-C, Huang, W.-Q. Wu, H.-H. Ho, K.-H. Chen, *IEEE T. Power Electr.* 25, 719(2010).
15. Y.-J. Lee, A. Knaligh, A. Chakraborty, and A. Emadi, *IEEE T. Power Electr.* 24, 1267 (2009).
16. R.-Y. Kim and J.-S. Lai, *IEEE T. Power Electr.* 23, 2310 (2008).
17. R.-Y. Kim, J.-S. Lai, *IEEE 23th Applied Power Electronics Conference and Exposition.* (2008), pp. 1754-1760.
18. H. Nagayoshi, T. Nakabayashi, H. Maiwa, and T. Kajikawa, *J. Electron. Mater.* 40, 657 (2011).
19. R.-Y. Kim, J.-S. Lai, B. York, and A. Koran, *IEEE T. Ind. Electr.* 56, 3709 (2009).
20. S. Kim, S. Cho, N. Kim, N. Baatar, and J. Kwon, *J. Electron. Mater.* 40, 867 (2011).
21. J. Park and S. Kim, *J. Electron. Mater.* 41, 1242 (2012).